

A low diffraction laser beam as applied to polymer ablation

Xuanhui Lu,^{a)} Y. Lawrence Yao,^{b)} and Kai Chen

Department of Mechanical Engineering, Columbia University, 220 Mudd Building, MC 4703, New York, New York 10027

(Received 9 January 2001; accepted for publication 3 August 2001)

A low diffraction beam is obtained by altering the existing resonator of a CO₂ laser using a special phase plate. The phase plate is designed based on the boundary diffraction principle and is implemented on the resonator rear mirror. It is found that the low diffraction beam has a smaller M^2 value than that of a Gaussian beam. The effects of the improved beam quality on a laser ablation process are investigated using a polymeric material. A theoretical model is provided to predict the laser ablated hole profile and penetration depth. The theoretical results are in agreement with the experimental measurements. Both the experimental and theoretical results show that the low diffraction beam has marked advantages over the Gaussian beam in ablation-dominated material removal processes in terms of larger depth and smaller taper at the same average power level.

© 2001 Laser Institute of America.

Key words: low diffraction, laser beam, CO₂ laser, laser drilling

I. INTRODUCTION

Laser beam quality plays an important role in quality and efficiency of laser materials processing applications. Higher beam quality typically means nearly fundamental-mode oscillation. Many efforts have thus been made to change high-order modes into the fundamental modes. The fundamental-mode Gaussian beam (i.e., TEM₀₀ or transverse electromagnetic mode) has long been regarded as an ideal beam, or diffraction-limited beam. The beam quality can be described quantitatively in term of M^2 as defined by Siegman.¹ A product of the standard deviation of the beam size and that of the divergence is formed. M^2 is the ratio of the product for a nondiffraction-limited, multitransverse-mode beam, to that of a Gaussian beam. The M^2 for the fundamental-mode Gaussian beam is thus unity. An interesting question is whether or not it is possible for a practical beam to have an M^2 value smaller than that of the fundamental-mode Gaussian beam. The concept of a low-diffraction beam having $M^2 < 1$ has been proposed.^{2,3} In other words, the low-diffraction beam has a higher central intensity and smaller divergence than a Gaussian beam.

The next question is whether the low-diffraction beam, whose M^2 value is smaller than that of a Gaussian beam, will translate into better quality and efficiency in laser materials processing applications, such as laser machining. Although it is generally agreed that the laser beam quality has a direct effect on machining quality, no consensus has been reached that a smaller M^2 is always beneficial to a machining process, because the machining process is a complicated thermal process that could also involve fluid flow and melt rejection. A beam with a smaller M^2 value is likely to result in smaller hole sizes or narrower slots, which is not in favor of melt

rejection. However, in an ablation-dominated laser machining process, most of the material is vaporized almost instantly and is removed mainly by vapor pressure. The low diffraction laser beam with a smaller M^2 value is thus expected to have beneficial effects on the ablative machining process.

The quality and profile of laser made holes, grooves, and cuts are obviously of importance, especially in the growing microelectronic and precision medical device industry.⁴⁻⁶ The quality is generally gauged by wall definition, extent of heat-affected zone, and ability to produce features with higher aspect ratio. Laser ablation of polymeric materials using laser beams is a well-established process and examples are found in Refs. 7 and 8. Factors of laser beams likely to affect drilling and grooving have been studied in many reports.^{9,10} This article presents the principles behind generation of a low diffraction beam and its applications to ablation-dominated drilling and grooving processes involving polymer material. Its beneficial effects on process quality are investigated in comparison with a Gaussian beam.

II. THE PRINCIPLE AND GENERATION OF LOW DIFFRACTION BEAM

The low diffraction beam is based on the boundary diffraction principle.^{2,3} The principle and generation of the beam is briefly summarized in this section. An advantage of the beam is that it can be obtained by altering the existing resonator of a CO₂ laser through a special phase plate implemented at the resonator rear mirror (Fig. 1).

Huygens suggested that every point on a wave front should be considered a new source of forward directed spherical waves. Extending this idea to interference, Fresnel developed what is considered the Huygens-Fresnel principle.¹¹ Kirchhoff provided a physical basis for this principle through the development of the Kirchhoff integral theorem, which treats scalar waves and is firmly based on the

^{a)}Also with: Department of Physics, Zhejiang University, China.

^{b)}Corresponding author; electronic mail: YLY1@columbia.edu

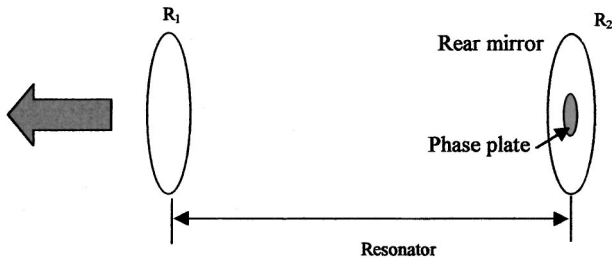


FIG. 1. Schematic of resonator configuration (with a half phase plate attached on the rear mirror inside laser cavity) to realize the low diffraction beam.

wave theory through the Helmholtz wave equation. For a spherical or plane monochromatic wave $U^{(i)}(Q)e^{-i\omega t}$ incident on an aperture A in a plane black screen, the diffraction field can be obtained by Kirchoff's formula,¹¹ as

$$U(P) = -\frac{1}{4\pi} \iint_A \left\{ U^{(i)}(Q) \frac{\partial}{\partial n} \left(\frac{e^{ikm}}{m} \right) - \frac{e^{ikm}}{m} \frac{\partial U^{(i)}(Q)}{\partial n} \right\} dm, \tag{1}$$

where m denotes the distance from a typical point in the aperture to the observation point P , k is the propagation constant of the incident wave, that is, $2\pi/\lambda$, and $\partial/\partial n$ denotes differentiation with respect to the normal of the surface of integration, pointing to the half-space containing the point P . The results obtained from Eq. (1) are in agreement with most experiments. In deriving Eq. (1), Kirchoff set on A :

$$U = U^{(i)} \quad \frac{\partial U}{\partial n} = \frac{\partial U^{(i)}}{\partial n}$$

on B :

$$U = 0, \quad \frac{\partial U}{\partial n} = 0, \tag{2}$$

where B denotes the portion of the nonilluminated side of the screen (area out of A). Equation (2) is the Kirchoff's boundary condition and is the basis of Kirchoff's diffraction theory.

According to Huygens' construction, every point of a wave front may be considered as a center of a secondary disturbance which gives rise to a spherical wavelet, and the wave front at any later instant can be regarded as the envelope of these wavelets. Fresnel was able to account for diffraction by supplementing Huygens' theory in postulating that the secondary wavelets mutually interfere, resulting in the so called Huygens-Fresnel principle.¹¹ According to the Huygens-Fresnel principle, Kirchoff proposed the following expression for the diffraction field:

$$U(P) = -\frac{iA}{2\lambda} \iint_A \frac{e^{ik(l+m)}}{lm} [\cos(n,l) - \cos(n,m)] dm, \tag{3}$$

where l is the distance between source and the edge of the aperture.

It is well known that the Sommerfeld's solution of the half-plate diffraction problem can be rigorously split into a

geometric optical wave and a diffraction wave. Later in 1917, an exact splitting of the Kirchoff's integral was obtained by Rubinowicz¹¹ for the case of an incident spherical or plane wave, and the boundary wave can be expressed as an integral along the edge of an aperture. For the case of a spherical wave normally incident upon a circular aperture, the optical field at the observation point P can be written as

$$U(P) = U^{(g)}(P) + U^{(d)}(P), \tag{4}$$

where $U^{(g)}(P)$ represents the disturbance as predicted by geometrical optics, given by

$$U^{(g)}(P) = \begin{cases} e^{ikL}/L, & \text{when } P \text{ is in the direct beam} \\ 0, & \text{when } P \text{ is in the geometrical shadow} \end{cases} \tag{5}$$

and L is the distance from the optical source to P . $U^{(d)}(P)$ represents the effect of diffraction which can be expressed as an integral over the edge of the diffraction aperture

$$U^{(d)}(P) = \frac{1}{4\pi} \oint_{\Gamma} \frac{e^{ik(l+m)}}{lm} \eta dh, \tag{6}$$

where Γ denotes the edge of an aperture, and η is an inclination factor.

It can be shown that when the axial observation point P is in the direct beam, $\eta < 0$. This means that there is a π phase jump between the boundary wave and the incident wave. Because the observation point P is always in the direct beam, according to the above analysis the π phase jump exists in most cases, especially for axial points. It is also valid when a convergent spherical wave or plane wave is normally incident upon a circular aperture. A new laser cavity, which generates a low diffraction beam, is proposed based on the recognition of the π phase jump.

According to the boundary diffraction wave theory, the far-field intensity distribution of the diffraction wave is formed by interference between two beams. One is the beam that passes directly through the aperture which propagates under the geometrical rule (geometrical beam), and the other is the beam produced by the boundary of the aperture (boundary beam). As mentioned above, the boundary wave possesses a phase jump of π compared with the incident beam. If the π phase is added to the geometrical beam, the geometrical beam will have the same phase as the boundary beam. This can be achieved by attaching a half phase plate to the rear mirror (Fig. 1). The interference of these two beams will form a new beam with a higher central intensity and higher directionality than the incident beam. If the incident beam is an ideal Gaussian beam, the output beam will have a better beam quality than the Gaussian beam.

III. CHARACTERIZATION OF LOW DIFFRACTION BEAM

Because the output of the low diffraction beam is not a Gaussian distribution, it is more practical to use the definition of 86.5% power content to measure the beam size. In

order to compare the beam quality of this new mode with the Gaussian mode, the equivalent beam quality factor M_e^2 is defined as follows:

$$M_e^2 = W_{86.5} \theta_{86.5} \frac{\pi}{\lambda}, \quad (7)$$

where $W_{86.5}$ is the equivalent beam waist size with 86.5% power content, $\theta_{86.5}$ is the divergence angle corresponding to the 86.5% power content, and λ is the beam wavelength.

The intensity distribution of Gaussian beam $I_0^G(r)$, and the low diffraction beam $I_0^L(r)$ at the beam waist can be written as

$$\begin{aligned} I_0^G(r) &= I_0 \exp\left(-\frac{2r^2}{W_0^2}\right) \\ I_0^L(r) &= I_0 \exp\left(-\frac{2r^2}{W_0'^2}\right) = I_0 \exp\left(-\frac{2r^2}{M_e^2 W_0^2}\right), \end{aligned} \quad (8)$$

where W_0 is the Gaussian beam waist radius, W' equals $M_e W_0$, and I_0 is the peak intensity. The intensity distribution at the far field can be obtained by using the beam propagation law, i.e., the ABCD law¹²

$$\begin{aligned} I_z^G(r, z) &= I_1 \exp\left[\frac{-2r^2}{W_0^2(1+z^2/z_r^2)}\right] \\ I_z^L(r, z) &= I_2 \exp\left[\frac{-2r^2}{W_0'^2(1+z^2/z_r^2)}\right] \\ &= I_2 \exp\left[\frac{-2r^2}{M_e^2 W_0^2(1+z^2/z_r^2)}\right], \end{aligned} \quad (9)$$

where z is the axial distance from the waist, and $z_r = \pi W_0^2/\lambda$ is the Rayleigh range.

The focal point radius for a Gaussian beam W_f^G is well known:¹³

$$W_f^G = \frac{\lambda f}{\pi W_z}, \quad (10)$$

where λ is wavelength, f is lens focal length, and W_z is original unfocused beam radius. The depth of focus for a Gaussian beam h_G is briefly derived below.

According to Gaussian beam properties its beam radius, at any distance along the beam path z from the waist, is given from the basic propagation equation

$$W(z) = W_0 \left[1 + \left(\frac{z}{z_r} \right)^2 \right]^{1/2}. \quad (11)$$

The depth of focus is normally defined as the distance between two points slightly away from the beam waist and the beam radius at these points is about 5% above the beam waist radius. By substituting $W(z) = 1.05W_0$ into Eq. (11), the depth of focus is obtained as

$$h_G = \frac{0.64\lambda}{\pi} \left(\frac{f}{W_z} \right)^2. \quad (12)$$

According to the M_e^2 definition [Eq. (7)], the focal point radius of a low diffraction beam of M_e^2 can be written as follows:

$$W_f^L = \frac{M_e^2 \lambda f}{\pi W_z}. \quad (13)$$

For the low diffraction beam, its Rayleigh range $z_r = \pi W_0^2/M_e^2 \lambda$. Then the focal depth of the low diffraction beam can be approximately represented as

$$h_L = \frac{0.64\lambda}{\pi M_e^2} \left(\frac{f}{W_z} \right)^2. \quad (14)$$

Compared to the focal point radius and the focal depth of a Gaussian beam, i.e., Eqs. (10) and (12), the focal point radius for the low diffraction beam is smaller than that of the Gaussian beam, while the focal depth for the low diffraction beam is larger than that of the Gaussian beam, since the M_e^2 value for the low diffraction beam is less than unity.

IV. THEORETICAL MODEL TO PREDICT ABLATIVELY DRILLED HOLE PROFILE

Under the irradiation of the laser beam, the material is first heated from room temperature to the melting temperature at which point melting takes place. Depending on the laser intensity and material properties, the molten material is evaporated by additional heating when it reaches the vaporization point and a vapor-filled keyhole is formed. Numerous models of laser drilling have also been developed. Paek and Gagliano¹⁴ developed a theoretical model to predict the temperature profile assuming a laser beam of circular cross section and uniform intensity. Dabby and Paek¹⁵ calculated the transient temperature and penetrating velocity during the vaporization process. A simple analytical model developed by Andrews and Atthey¹⁶ was used to predict the penetrating hole profile from a high-intensity beam ablation. The model is based on the hydrodynamic force balance on the liquid surface melted by the laser beam. The laser energy absorbed at the surface causes vaporization of the metal. There are four forces that are taken into account: recoil pressure, gravity, surface tension, and vapor pressure. The recoil pressure is caused by vaporizing the metal so that it undergoes a momentum change, and is primarily responsible for maintaining a depression in the material. The recoil pressure is obtained through vapor velocity, which can be calculated through energy balance. The effects of hole geometry are incorporated into the force and energy balance. The details of the model are described in the Appendix. In the model, the incident beam power is assumed to be uniformly absorbed at the surface for the same incident angle, i.e., the absorption coefficient is assumed to be geometry independent. The vapor pressure inside the hole is assumed to be equal to the atmospheric pressure. In reality, the beam absorption may not be uniform due to surface irregularity, and the process is complicated by compressible vapor flow and plasma.

To solve the nonlinear partial differential equation, Eq. (A7) with boundary conditions Eq. (A8) in the Appendix, the independent variable S is first transformed by an exponential parameter so that the region of interest ($0 < S \leq \infty$) is trans-

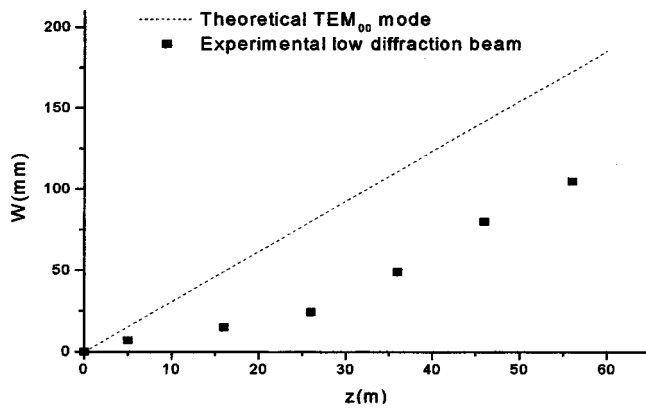


FIG. 2. Beam radius of the measured low diffraction beam and theoretical TEM_{00} mode vs axial distance between the output coupler to the measurement location.

formed to a finite region $(0,1]$. The finite-difference method is then used to solve the nonlinear problem. The finite region is divided into many equal subintervals and the single equation becomes a nonlinear matrix system. Newton's method for a nonlinear system is then used to approximate the solution to the system. The process is repeated until satisfactory convergence is achieved.

In comparison, for convenience the constant coefficient of the normalized power density $Q(R)$ in Eq. (A7) is calibrated so that the hole depth approximately matches the experimental hole depth. The model predicts the hole profile in the same way for both the Gaussian beam and the low diffraction beam except for using different values for their peak I_0 and the waist beam radius W_0 in Eq. (A7).

V. EXPERIMENT CONDITIONS

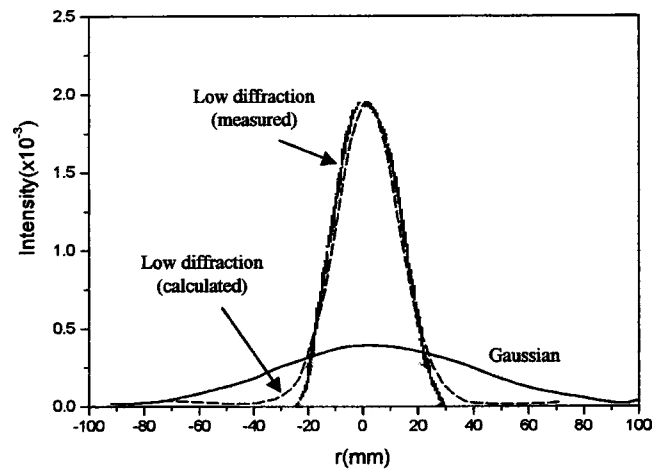
Experiments were carried out on a CO_2 laser with maximum average power of 12 W. The original resonator of the laser system generates a fundamental mode Gaussian beam (i.e., TEM_{00}). According to the principle described above, an identical resonator is modified with its structure as schematically shown in Fig. 1 to generate a low diffraction beam. The intensity profile and divergence of the low diffraction beam are measured. Both beams are used to ablate acrylic. Experimental conditions are kept the same for both cases. The laser operates in continuous wave mode. Hole diameter, depth, and taper are measured. Both beams are also used to groove the same material.

Unfocused beams are used to imprint acrylic within the power range of 7–9 W and ablation time of 0.8–1 s. Focused beams are then used to drill on the same material, in the power range of 7–9.2 W and ablation time of 0.6–2 s. The focal point with respect to the workpiece was varied by about 1 mm to compare its effect on drilling results from both beams. The focused beams finally are applied to grooving on the same material.

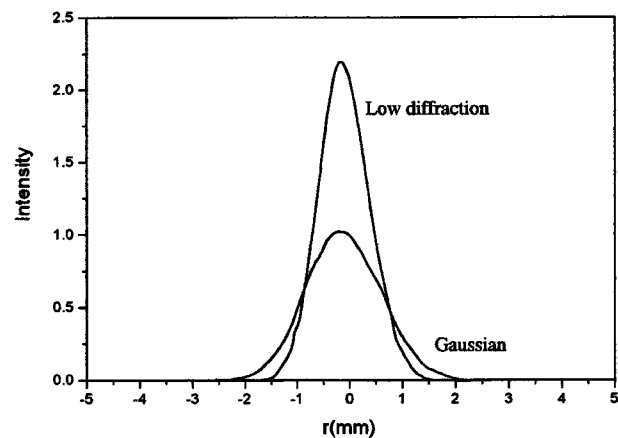
VI. COMPARATIVE RESULTS AND DISCUSSION

A. Beam characterization

Figure 2 shows experimental results of beam radius of



(a) Far field



(b) Near field

FIG. 3. Intensity distributions [Calculations are based on Eqs. (8) and (9), with $W_0=1.49$ mm (experimentally measured) and $M_e^2=0.3$ [using Eq. (7)]: (a) far field and (b) near field.

the low diffraction beam at various distances. It is seen that the divergence angle of the low diffraction beam is smaller than that of the theoretical TEM_{00} mode. Based on experimentally measured $W_{86.5}$ and $\theta_{86.5}$, and $\lambda=10.6$ μm for the CO_2 laser, the equivalent beam quality factor $M_e^2 \cong 0.3$ is obtained.

The intensity profile of the low diffraction beam in the far field is experimentally measured and superposed in Fig. 3(a) with the calculated intensity profiles of both the low diffraction and Gaussian beam according to Eq. (9). As seen, there is a good agreement between the experimental and calculated profiles, and the low diffraction beam has a much higher central intensity and smaller divergence than that of the Gaussian beam. Using Eq. (8), the near-field intensity profiles of both beams are plotted in Fig. 3(b). It can be seen that the low diffraction beam in the near field also has a higher central intensity and smaller diameter than the Gaussian beam.

B. Comparison of theoretical and experimental results

Figure 4 shows imprints made on acrylic by an unfocused Gaussian beam and low diffraction beam when the

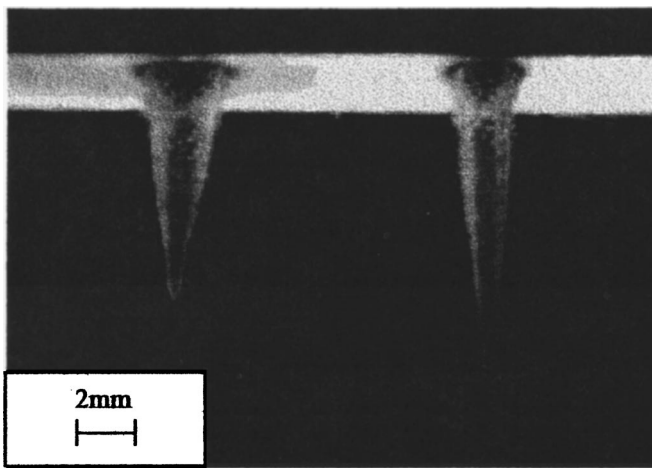


FIG. 4. Acrylic imprints with Gaussian (left) and the low diffraction beam (right) (9 W, 1 s, both unfocused).

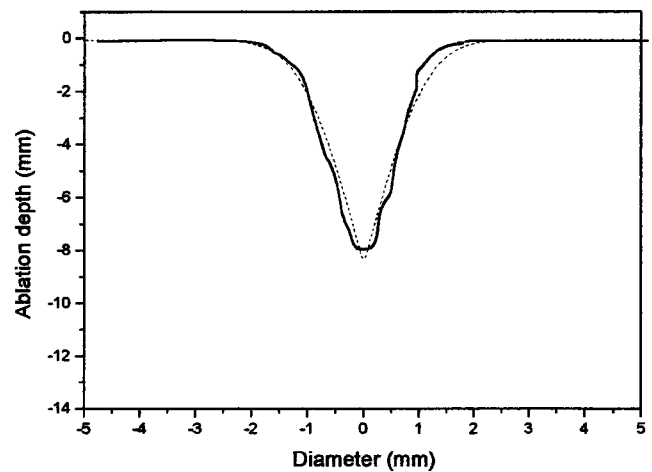
average power is 9 W and ablation duration is 1 s. Although the power level is the same, the low-diffraction beam has a higher energy intensity and a smaller beam size. Not surprisingly, the hole profiles closely follow that of beams in the ablative machining process. Cross sections of the profiles are also shown in solid lines in Fig. 5 to compare with the theoretically calculated ablation profiles in dotted lines.

The theoretically calculated ablation profiles are obtained as outlined in Sec. IV and in the Appendix. The energy density and the beam size for both the low diffraction beam and Gaussian beam are experimentally obtained and used in the theoretical model to predict the hole profile as shown in Fig. 5 in dotted lines. For both beams, the average power is set as 9 W. The waist radius for the resonator generating the Gaussian beam is measured as $W_0 = 1.49$ mm, while for the resonator generating the low diffraction beam the beam radius is measured as $W'_0 = 0.75$ mm. As a result, the intensity is 129 W/cm^2 at the waist for the Gaussian beam, and 509 W/cm^2 at the waist for the low diffraction beam. The theoretical predication agrees with experimental results.

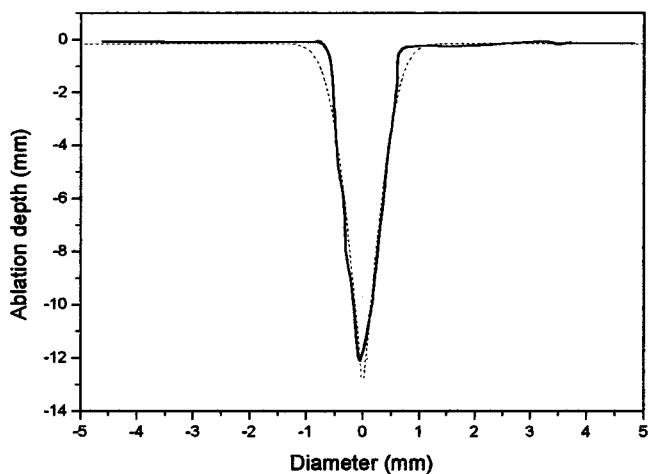
The simple analytical model used for the calculation is based on force and energy balance on the hole surface and does not take transient phenomena into account. The calculation is thus time independent. This is only applicable for relatively long drilling times in which the hole depth remains unchanged with time. The laser ablation process is often accompanied by plasma and shock waves depending on the laser intensity. Despite the simplifications, the model captures the basic features at the end of ablation as seen from Figs. 5 and 6.

There is some discrepancy at the top part of the hole profiles under the condition of the low diffraction beam [Fig. 5(b)]. The reason is that beam intensity in the theoretical model is based on a deformed Gaussian beam of optical beam quality factor M_e^2 , while the actual beam is obtained based on the boundary diffraction principle.

The beams are then focused using a lens with a focal length of 40 mm. The CO_2 laser varies at two average power levels: 7 and 9.2 W. For the Gaussian beam, the resultant



(a) With Gaussian beam



(b) With the low diffraction beam

FIG. 5. Theoretical (dashed line) and experimental results (solid line) of hole profiles (power=9 W, duration=1 s, unfocused, acrylic): (a) with Gaussian beam and (b) with the diffraction beam.

average power intensity is $5.22 \times 10^4 \text{ W/cm}^2$ for 7 W, and $6.71 \times 10^4 \text{ W/cm}^2$ for 9.2 W. For the low diffraction beam, the resultant average power intensity is $2.01 \times 10^5 \text{ W/cm}^2$ for 7 W, and $2.68 \times 10^5 \text{ W/cm}^2$ for 9.2 W.

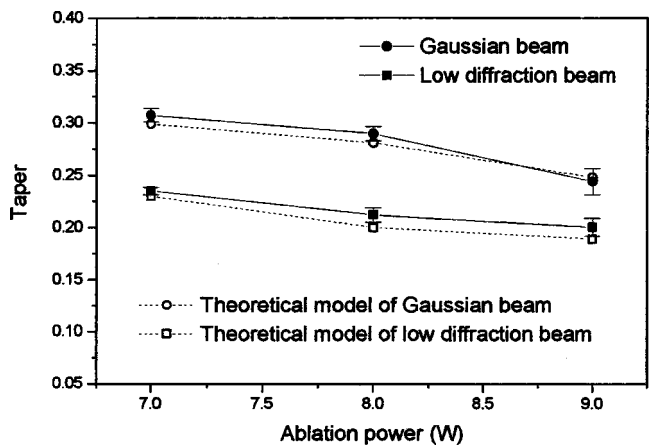


FIG. 6. The hole taper vs ablation power (ablation duration=0.8 s, focused, acrylic).

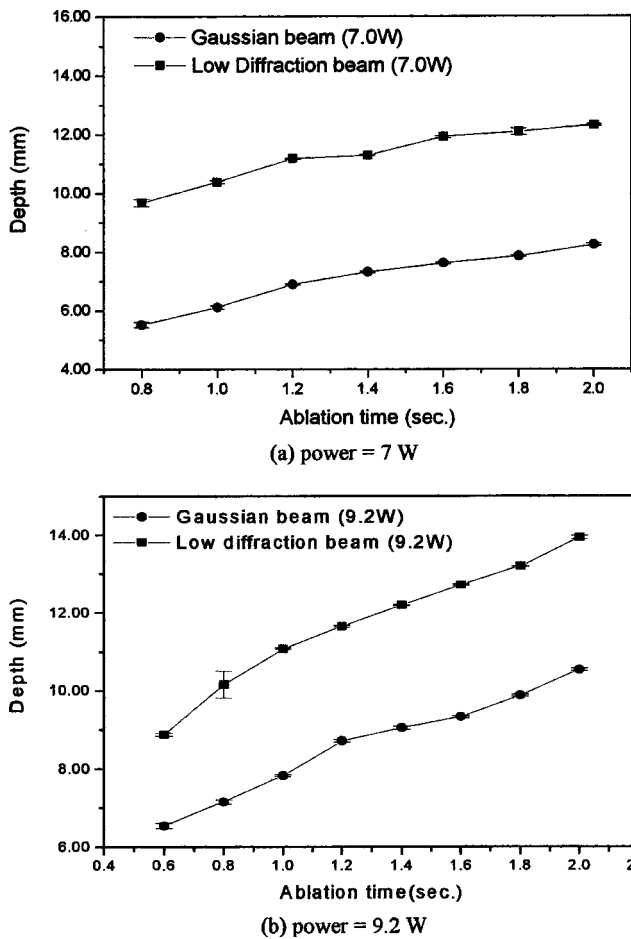


FIG. 7. Drilling depth by both the Gaussian beam and the low diffraction beam vs ablation duration (focused, acrylic): (a) power=7 W and (b) power=9.2 W.

Figure 6 shows the variation of hole taper against ablation power for both the low diffraction beam and Gaussian beam. Taper is defined as the ratio of hole diameter to hole depth (therefore is the inverse of aspect ratio) and is one of the quality factors for the hole profile. It is seen from Fig. 6 that the hole drilled with the low diffraction beam has significantly smaller taper values than the hole drilled with the Gaussian beam. The predicted values from the theoretical model are also shown in the figure and are generally in agreement with the measured values. The taper value decreases with increasing power level for both low diffraction beam and Gaussian beam. This is because the diameter of the hole increases much slower than the hole depth when the power level increases, as seen from Figs. 7 and 8.

C. Parametric studies

Figure 7 shows the measured drilling depth versus ablation time at two power levels. The hole depth drilled with the low diffraction beam is much larger than that with the Gaussian beam because of the higher central energy intensity at the same average power level. The depth with the low diffraction beam is about 40% higher than that with the Gaussian beam under the condition used.

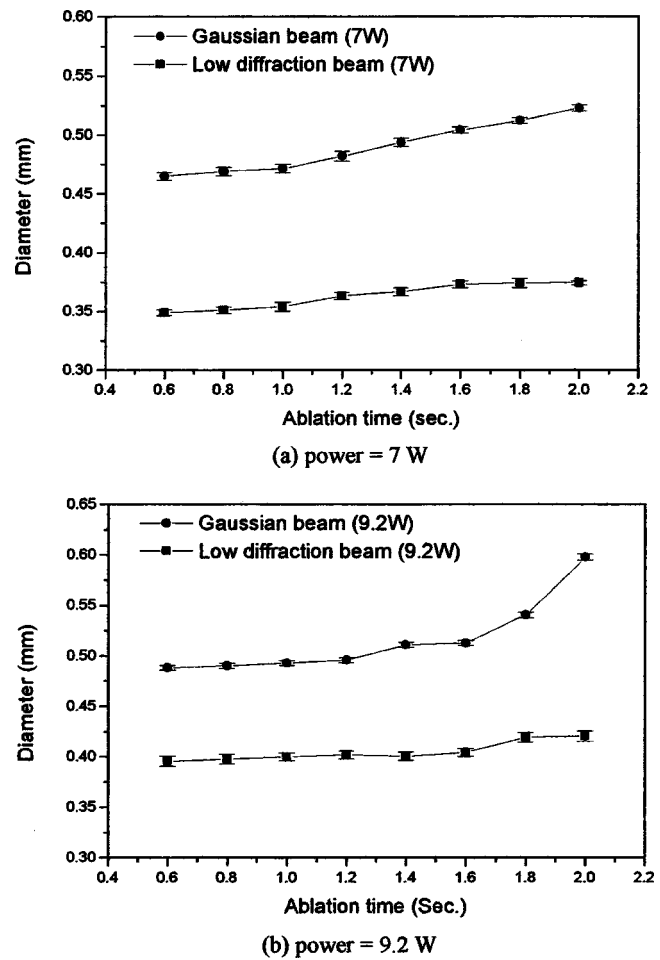


FIG. 8. The drilled hole diameter vs ablation time with both the Gaussian beam and the low diffraction beam (focused, acrylic): (a) power=7 W and (b) power=9.2.

Figure 8 shows the measured diameter of the drilled hole versus ablation time at two power levels. It is seen that the hole diameter drilled with a low diffraction beam is about 25% smaller than that with a Gaussian beam. In addition, with the ablation time increasing, the drilled hole diameter with the low diffraction beam increases slower than that with the Gaussian beam, especially at longer ablation times clearly because the low diffraction beam has smaller divergence and longer focal depth.

It is theoretically shown in Sec. III that the low diffraction beam has a longer focal depth than that of a Gaussian beam. Figure 9 shows experimental results with ablation power of 7 W and ablation duration of 0.5 s. In Fig. 9, L represents the distance from the focusing lens to the top surface of the workpiece. As seen in Fig. 9(a), the ablation hole diameter drilled with the low diffraction beam changes from about 0.3 to 0.7 mm, while the hole diameter drilled with the Gaussian beam changes from 0.4 to 1.0 mm, when L changes by the same amount, i.e., about 1 mm.

From Fig. 9(b), it is seen that the hole depth near the focal point [corresponding to the minimum hole diameter as seen in Fig. 9(a)] varies slower for the low diffraction beam than for the Gaussian beam. This is again desirable, especially when thick section machining is concerned.

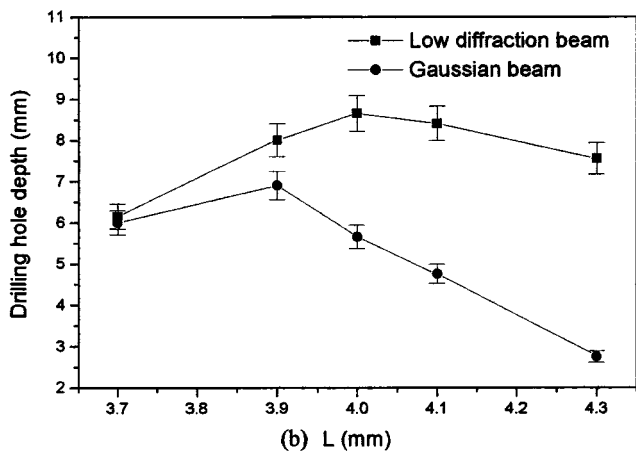
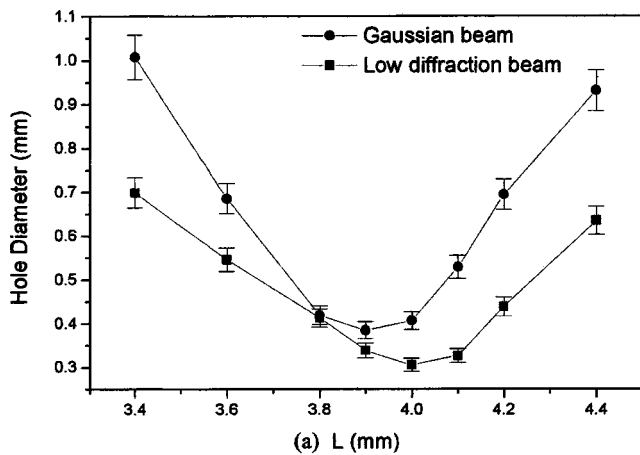


FIG. 9. (a) Hole diameter and (b) hole depth vs the distance from focus lens to workpiece top surface (power=7 W, duration=0.5 s).

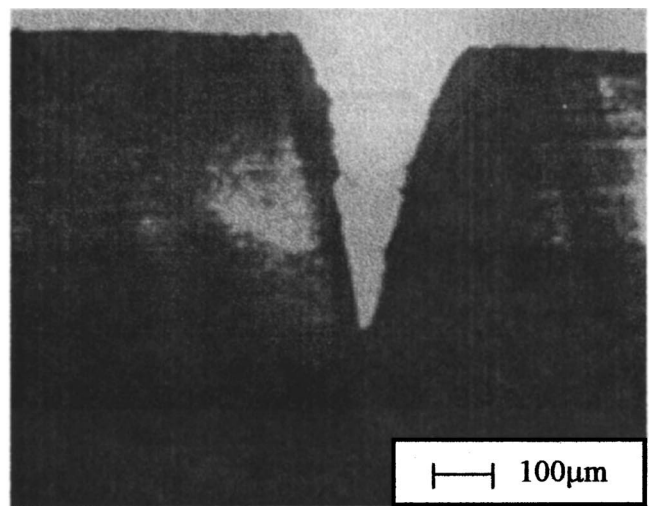
D. Grooving

The focused low diffraction beam and Gaussian beam are applied to grooving the same material. Figure 10 compares the cross sections of groove profiles ablated by both beams. It is seen that at the same power level (9 W) and the grooving speed (14 mm/s), the cross sectional profile with the low diffraction beam has a higher aspect ratio than that with the Gaussian beam.

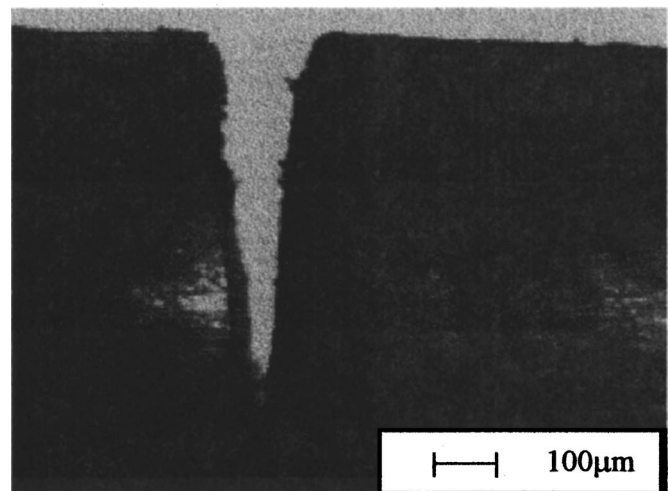
It is seen that the beneficial effects of the low diffraction beam in drilling extend to applications such as grooving and likely cutting as well. These beneficial effects include a higher aspect ratio and lower sensitivity to focal point location. They are expected to be more significant at higher power levels. While this article only covers acrylic, other materials are expected to have similar beneficial effects when ablated by the low diffraction beam because during ablative laser machining, machined profiles chiefly rely on the optical beam quality. When the power intensity is below the ablation threshold of a material, other factors also play a significant role.

VII. CONCLUSION

A low diffraction beam, which has a M^2 factor smaller than unity, is implemented with a low power CO₂ laser and applied to ablation-dominated drilling and grooving of



(a) Groove cross section with Gaussian beam



(b) Groove cross section with low diffraction beam

FIG. 10. Typical groove profiles with Gaussian beam and the low diffraction beam (power=9 W, speed=14 mm/s, both focused, acrylic): (a) groove cross section with Gaussian beam and (b) groove cross section with low diffraction beam.

acrylic. The experimental results show that the low diffraction beam produced larger depth, smaller taper, and smaller hole diameter, as compared with a Gaussian beam at the same average power level. This is true for both the unfocused and focused cases. The focal depth of the focused low diffraction beam is also longer than the Gaussian beam, indicating its suitability for processing thick sections of material. Similar results are obtained when the beam is applied to grooving applications. A simple ablation model is used to predict the hole profile generated by both a Gaussian beam and the low diffraction beam, and the theoretical results are in agreement with the experimental observations. If the implementation of the low diffraction beam is extended to a higher power level laser system, the above mentioned beneficial effects will be more significant. For other materials, as long as ablation is the dominant mechanism of material removal, similar beneficial effects can be expected. In cases

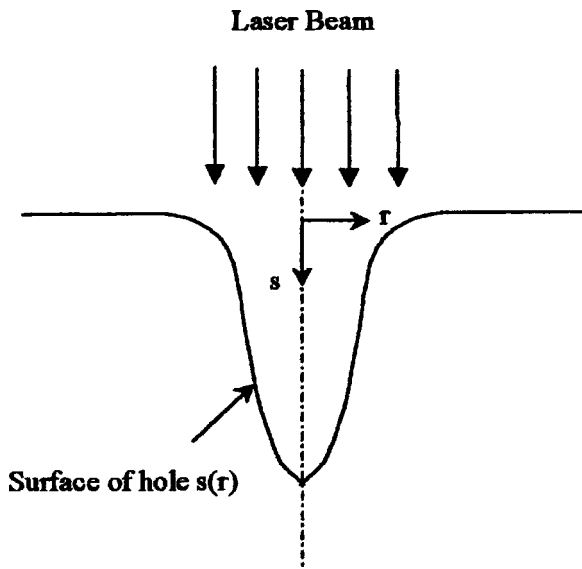


FIG. 11. Schematic of the drilling model.

where ablation is not dominant, the low diffraction beam is likely to offer at least some of the advantages but further studies are needed.

ACKNOWLEDGMENTS

The financial support provided via a Pao Scholarship and Columbia University is gratefully acknowledged.

APPENDIX

A simple analytic model (Fig. 11) to estimate the hole profile is presented as follows.¹⁶ The model assumes that all of the incident power is absorbed and is used to evaporate the surface (neglecting heat conduction). The vapor pressure effects are not considered.

Bernoulli's equation gives

$$\frac{1}{2} v^2 + \frac{p}{\rho} + gs = 0 \tag{A1}$$

for any streamline of the flow, where v , p , and ρ are the liquid velocity, pressure, and density, respectively. The above equation takes the atmospheric pressure to be zero and $s = 0$ to be the level of the undisturbed liquid, i.e., $v = 0$. From the dynamic condition at the surface, we have

$$p + \gamma/C = \rho_g v_{gn}^2 - \rho v_n^2 \tag{A2}$$

where γ is the surface tension and C is the curvature of the hole surface. The subscript g and n refer to the gas and the normal component of velocity, respectively. From

$$\rho v_n = \rho_g v_{gn}$$

and

$$\rho_g / \rho \ll 1$$

we have

$$p \approx (\rho v_n)^2 / \rho_g - \gamma/C. \tag{A3}$$

By substitution in Eq. (A1), neglecting $\frac{1}{2}v^2$ in comparing with $(\rho v_n)^2 / \rho_g$, and calculating the curvature, we obtain

$$\frac{\rho v_n^2}{\rho_g} + gs - \frac{\gamma}{\rho} \left\{ \frac{s''}{(1+s'^2)^{3/2}} + \frac{s'}{r(1+s'^2)^{1/2}} \right\} = 0. \tag{A4}$$

From conservation of energy, the absorbed laser power equates the vaporization energy, that is,

$$I_0(r) \cos \theta = \rho v_n h, \tag{A5}$$

where θ is the angle between the beam direction and the surface normal direction, and h is the energy per unit mass needed to vaporize the liquid. From the geometry relation

$$\cos \theta = (1 + s'^2)^{-1/2}, \tag{A6}$$

we have $v_n = I(r)h(1 + s'^2)^{-1/2}$. Substituting it into Eq. (A4), and normalizing the equation, the equation for the shape of the hole is obtained:

$$T \left\{ \frac{d^2 S}{dR^2} + \frac{1}{R} \left(1 + \left(\frac{dS}{dR} \right)^2 \right) \frac{dS}{dR} \right\} - S \left(1 + \left(\frac{dS}{dR} \right)^2 \right)^{3/2} = Q^2(R) \left(1 + \left(\frac{dS}{dR} \right)^2 \right)^{1/2}, \tag{A7}$$

where

$$R = r/W_0, \quad S = s/W_0, \quad T = \frac{\gamma}{\rho g W_0^2},$$

$$Q(R) = \frac{I_0(r)}{(g \rho \rho_g h^2 W_0)^{1/2}}.$$

W_0 is some characteristic width of the beam.

Equation (A7) is a second-order differential equation with two boundary conditions specified as:

$$\frac{dS}{dR} = 0, \quad \text{at } R = 0;$$

and

$$S \rightarrow 0, \quad \text{as } R \rightarrow \infty. \tag{A8}$$

¹A. E. Siegman, "Defining and measuring laser beam quality," in *Solid State Laser-New Developments and Applications*, edited by M. Inguscio and R. Wallenstein (Plenum, New York, 1993), pp. 13–28.
²S. Wang, X. Lu, C. Pan, and S. Yu, "A new beam CO₂ laser," *Optik (Stuttgart)* **101**, 32 (1995).
³S. Wang *et al.*, "A new beam produced by CO₂ laser," *Optik (Stuttgart)* **101**, 84 (1995).
⁴B. S. Yibas, "Study of affecting parameters in laser hole drilling of sheet metals," *ASME J. Eng. Mater. Technol.* **109**, 282–287 (1987).
⁵R. W. Olson and W. C. Swope, "Laser drilling with focused Gaussian beams," *J. Appl. Phys.* **72**, 3686–3696 (1993).
⁶H. Rohde and F. Dausinger, "The forming process of a through hole drilled with a single laser pulse," *Proceedings ICALEO'95*, 1995, pp. 331–340.
⁷I. Miyamoto and H. Maruo, "The mechanism of laser cutting, welding in the world," *J. Int. Instit. Welding* **29**, 283–294 (1991).
⁸T. F. Redmond, J. R. Lankard, J. G. Balz, G. R. Proto, and T. A. Wassick, "The application of laser process technology to thin film packaging," *IEEE Trans. Compon., Hybrids, Manuf. Technol.* **16**, 6–12 (1993).
⁹J. J. Batteh, M. M. Chen, and J. Mazumder, "Scaling and numerical analysis of pulsed laser drilling," *Proceedings ICALEO'98*, 1998, paper B-30.

- ¹⁰J. Powell, *CO₂ Laser Cutting* (Springer, New York, 1993).
- ¹¹M. Born and E. Wolf, *Principles of Optics*, 6th ed. (Pergamon, New York, 1980), Chap. 8.
- ¹²H. Kogelnik and T. Li, "Laser beams and resonators," *Appl. Opt.* **5**, 1550 (1966).
- ¹³S. A. Collins, "Lens-system diffraction integral written in term of matrix optics," *J. Opt. Soc. Am.* **60**, 1168–1177 (1970).
- ¹⁴U.-C. Paek and F. P. Gagliano, "Thermal analysis of laser drilling processes," *IEEE J. Quantum Electron.* **QE-8**, 112–119 (1972).
- ¹⁵F. W. Dabby and U.-C. Paek, "High-intensity laser-induced vaporization and explosion of solid material," *IEEE J. Quantum Electron.* **QE-8**, 106–111 (1972).
- ¹⁶J. G. Andrews and D. R. Atthey, "Hydrodynamic limit to penetration of a material by a high-power beam," *J. Phys. D* **9**, 2181–2194 (1976).